Cavitation Thermometry Using Molecular and Continuum Sonoluminescence

Lawrence S. Bernstein* and Mitchell R. Zakin

Spectral Sciences, Inc., 99 South Bedford Street, Burlington, Massachusetts 01803

Edward B. Flint[†] and Kenneth S. Suslick

School of Chemical Sciences, University of Illinois at Urbana−Champaign, 505 South Mathews Avenue, Urbana, Illinois 61801

Received: December 8, 1995; In Final Form: January 26, 1996[⊗]

The use of molecular and continuum emission spectra from multiple bubble (MB) and single bubble (SB) sonoluminescence (SL) is explored as a probe of bubble temperature during cavitational collapse. It is proposed that molecular and continuum SL arise from different chemical pathways, which occur during discrete intervals along the cavitational collapse time line, thus yielding different cavitation temperatures. A coupled bubble dynamics/chemical kinetic model of cavitational collapse is developed and used to explore a variety of proposed molecular SL mechanisms for the C_2(d→a), CN(B→X), and OH(A→X) emissions. Molecular SL is shown to arise from chemiluminescent reactions of seed molecules (e.g., hydrocarbons, N_2, H_2O) and their dissociation products, and occurs during the early and middle stages of cavitational collapse. This emission is broadly characterized as originating from reactions involving singly or multiply bonded molecular precursors with corresponding effective emission temperature ranges of approximately 3000−8000 and 8000−25 000 K, respectively. An analysis of an experimentally observed CN(B→X) MBSL spectrum is reported which is consistent with CN emission occurring over a broad distribution of cavitation temperatures ranging from approximately 5000 to 15 000 K. Continuum SL is attributed to transitions of electrons produced by high-temperature ionization and confined to voids in the dense fluid formed during the latter stages of cavitational collapse. The continuum is similar for both SBSL and MBSL, and is characterized by a temperature range of ≈20 000−100 000 K. The observation of significant molecular emission for MBSL, and not for SBSL, is attributed to the broad distribution of initial bubble sizes for MBSL. In SBSL, a single bubble is repetitively cycled through collapse and reexpansion, and its collapse is driven well into the continuum emission regime. In MBSL, only a small fraction of the bubbles will be driven to this level of collapse, while a much larger fraction will attain only the single or multiple bond chemistry regimes. Thus in MBSL the bubble size distribution averaged emission will tend to enhance the molecular relative to the continuum emission. It is concluded that both SBSL and MBSL are consistent with an adiabatic compressional heating description of bubble collapse.

I. Introduction

The maximum temperature attained during cavitational collapse of gas bubbles formed when resonant acoustic energy is introduced into a liquid has been the subject of numerous experimental and theoretical investigations.[1−16] Depending on the experimental conditions and the spectra observed, temperature estimates of cavitational collapse have ranged from approximately 1000 to 10 000 000 K. For example, previous analyses of continuum single bubble sonoluminescence (SBSL) and molecular multiple bubble sonoluminescence (MBSL) spectra have yielded very different effective cavitation temperatures. Using the recently developed confined electron spectral model[8] for the strong continuum emission observed in SBSL,[7] Bernstein and Zakin[8] derived an effective continuum emission temperature of 35 000 ± 5000 K for Ar in H_2O. Previously, Flint and Suslick[3,4] demonstrated that MBSL from Ar in silicone oil produced C_2(d→a) Swan band molecular emission characterized by a much colder molecular emission temperature of 5075 ± 156 K. These very different temperatures have led to speculation that SBSL and MBSL may originate from different cavitational collapse mechanisms.[5,16,17] This interpretation is further supported by the dissimilar appearance of SBSL and MBSL spectra; SBSL spectra consist of only an emission continuum, while most MBSL spectra consist of one or more molecular band systems riding atop a strong continuum.

In this study, we will examine the use of molecular and continuum emission MBSL and SBSL spectra as a probe of bubble temperature during cavitational collapse, in order to gain insight into the dynamics of cavitational collapse temperatures associated with specific molecular and continuum emitters. We find that the effective temperature derived from analysis of a particular spectral feature reflects the cavitational collapse time interval during which the emitting species can exist; thus, such a temperature is strictly a lower bound to the maximum cavitational temperature. The large difference in effective temperatures cited above for molecular MBSL and continuum SBSL from Ar bubbles can be attributed to the much broader distribution of bubble collapse dynamics occurring in MBSL vs SBSL. Further, we believe that SBSL and MBSL spectra can be quantitatively explained with the *same* underlying *physical* mechanism: compressional heating from adiabatic cavitational collapse of the bubble wall.

In the remainder of this paper, a coupled bubble dynamics/chemical kinetic cavitational collapse model is used to explore these hypotheses via calculations of the temperature/temporal profiles of the key molecular emitters observed in MBSL. These

[†] Current address: Department of Chemistry, Bradley University, Peoria, IL.

[⊗] Abstract published in *Advance ACS Abstracts,* March 15, 1996.

0022-3654/96/20100-6612$12.00/0

include the C_2(d→a), CN(B→X), and OH(A→X) band systems.[3,4,9,18] In addition, cavitation temperatures are derived from new spectral analyses of previously observed CN(B→X) and continuum MBSL.

II. Model Description

A. Cavitational Collapse Dynamics. A simplified description of the adiabatic cavitational collapse dynamics was adopted for integration with a finite rate chemical kinetic model of the molecular chemiluminescent pathways, and is defined by

$$R = R_0 + (\mathrm{d}R/\mathrm{d}t)\Delta t \quad (1)$$

$$\rho = \rho_0(V_0/V) \quad (2)$$

$$\rho^* = \rho\sigma^3 \quad (3)$$

$$T = F(\rho^*) \quad (4)$$

where R is the time dependent bubble radius, dR/dt is the rate of contraction of the bubble radius, Δt is time measured relative to a reference radius R_0, V is volume, ρ is number density, ρ^* is reduced density, σ is the hard sphere diameter of the host gas, and the temperature T is a function of the reduced density. The dependence of T on ρ^* is based on an adiabatic collapse model, described in detail elsewhere,[8] which utilizes the Carnahan−Starling equation of state[19] because of its realistic treatment of dense fluids (i.e., $\rho^* \approx 1$ at the minimum bubble radius R_{min}), and includes the effect of excited electronic states on the specific heat ratio. The major simplification employed in this study is the use of a constant contraction velocity, dR/dt. A more rigorous approach would be to determine $R(t)$ from the Rayleigh−Plesset equation;[1] however, as discussed below, the salient features of the molecular emission chemistry do not depend strongly on the precise details of the time dependence of $R(t)$. In this model, R_0 is taken to be the radius of the initially formed bubble (i.e., the radius before the expansion phase), T_0 is the liquid temperature, and ρ_0 is determined from T_0 and the pressure head P_0. The initially formed bubble expands to a maximum radius R_{max} which is much larger than R_0; however, the initial stage of cavitational collapse from R_{max} to R_0 proceeds relatively slowly and isothermally and plays no role in the molecular and continuum emission chemistry. The collapse from R_0 to the minimum bubble radius R_{min} occurs much faster, attaining a maximum velocity approaching the speed of sound in the liquid, which for most liquids is between 1000 and 2000 m/s.

The bubble collapse dynamics model described above pertains to molecular SL produced during a *single* cavitational collapse. It is noted that molecular SL may also be produced during reexpansion of a bubble and its subsequent afterbounces.[13b] Additionally, for a stably cavitating bubble, the same parcel of gas undergoes many cavitational collapses; thus the bubble molecular composition will evolve over time and would be expected to be different from the molecular composition of gases dissolved in the liquid. Such complicating factors, however, are not expected to alter the general conclusions based on the simplified model.

B. Chemistry Overview. Before presenting calculations for specific mechanisms, it is useful to consider in a more general sense the major chemical pathways that are expected to control the production and quenching of the molecular emissions. The initial step involves the dissociation of the seed molecules (for discussion purposes a simple triatomic molecule ABC seeded into a rare gas is considered), which can proceed along two different reaction pathways,

$$\mathrm{ABC} \rightarrow \mathrm{AB} + \mathrm{C} \quad \text{(unimolecular decomposition)} \quad (5)$$

$$\mathrm{ABC} + \mathrm{M} \rightarrow \mathrm{AB} + \mathrm{C} + \mathrm{M} \quad \text{(collisional dissociation)} \quad (6)$$

Generally, larger polyatomic molecules undergo unimolecular decomposition, in which the rate of decomposition depends only on temperature and not on density. Smaller molecules, typically involving three or fewer atoms, tend to dissociate through collisions with a third body, M, making the dissociation rate both temperature and density dependent. If a sufficiently high temperature and density are attained during the collapse, these dissociation mechanisms will eventually lead to complete atomization of the seed molecule, ABC → → A + B + C. The chemiluminescent reactions fall into two categories,

$$\mathrm{A} + \mathrm{BC} \rightarrow \mathrm{AB}^* + \mathrm{C} \quad \text{(bimolecular reaction)} \quad (7)$$

$$\mathrm{A} + \mathrm{B} + \mathrm{M} \rightarrow \mathrm{AB}^* + \mathrm{M} \quad \text{(atom−atom recombination)} \quad (8)$$

Because bimolecular production of an excited state molecule AB* requires the presence of at least one diatomic or polyatomic reactant (BC in this example), it will turn off at lower temperatures than the atom−atom recombination mechanism (i.e., at higher temperatures the BC bond breaks before bimolecular reaction can occur). The temperature regime over which the BC bond dissociates depends on the strength of the bond; thus it is expected that bimolecular reactions involving single bonds will generally occur at substantially lower temperatures than reactions involving double and triple bonds. The observed emission intensity from AB* reflects a balance between its formation process, its radiative decay rate (i.e., the Einstein A coefficient), and its removal processes. These additional reactions are represented by

$$\mathrm{AB}^* \rightarrow \mathrm{AB} + h\nu \quad \text{(radiative decay)} \quad (9)$$

$$\mathrm{AB}^* + \mathrm{M} \rightarrow \mathrm{AB} + \mathrm{M} \quad \text{(collisional quenching)} \quad (10)$$

$$\mathrm{AB}^* + \mathrm{M} \rightarrow \mathrm{A} + \mathrm{B} + \mathrm{M} \quad \text{(collisional dissociation)} \quad (11)$$

The reactions described above represent a set of time dependent coupled differential equations which can be integrated using eqs 1−4 to specify the overall thermodynamic state of the collapsing bubble. This yields the time dependent concentration of all the atomic and molecular species, and thus determines the temperature regime for the various molecular emission species. The specific chemical mechanisms for producing the C_2, CN, and OH molecular emissions are summarized in Table 1.

III. Model Calculations and Spectral Analysis

A. C_2(d→a) SL Chemistry. Calculations were performed for conditions representative of those used by Flint and Suslick[4] for the observation of C_2 MBSL from Ar/silicone oil. In this case, $T_0 = 277$ K, $P_0 = 1$ atm, $R_0 = 10$ μm, and dR/d$t = 400$ m/s. The values selected for R_0 and dR/dt are estimates, and the sensitivity of the calculated C_2 emission to variation of these parameters is explored below. The source of C/H-containing species in this experiment was the silicone oil (polydimethylsiloxane = $[(CH_3)_2SiO]_n$). Due to the very low silicone oil vapor pressure, ≈0.01 Torr at 277 K, only a small mole fraction of C/H atoms ($\approx 10^{-4}$) is present in the Ar bubbles. After initial cleavage of the CH_3−Si bond, the chemistry giving rise to the C_2 emission involves only C/H-containing species. For simplicity, we ignore the Si/O chemistry and choose C_2H_6 (i.e., CH_3−CH_3) as an "equivalent" surrogate seed molecule. Use of larger saturated hydrocarbons as the surrogate is expected to produce similar results. The C_2 reaction mechanism and associated

TABLE 1: Summary of Chemical Reactions and Rate Constants[a]

	reaction	A[b]	N[c]	E (K)
	C_2 Emission Chemistry			
R1	$C_2H_6 \rightarrow CH_3 + CH_3$	1.2×10^{18}	1.79	4.58×10^4
R2	$CH_3 + M \rightarrow CH_2 + H + M$	1.0×10^{16}	0	4.56×10^4
R3	$CH_2 + M \rightarrow CH + H + M$	4.0×10^{15}	0	4.18×10^4
R4	$CH_2 + M \rightarrow C + H_2 + M$	1.4×10^{14}	0	2.97×10^4
R5	$CH + M \rightarrow C + H + M$	2.0×10^{14}	0	3.37×10^4
R6[d]	$C + CH_2 \rightarrow C_2(d) + H_2$	7.5×10^{13}	0	0
R7[e]	$C_2(d) + M \rightarrow C_2 + M$	6.0×10^{12}	0	0
	CN Emission Chemistry			
R8	$N_2 + M \rightarrow N + N + M$	5.6×10^{19}	2.5	1.13×10^5
R9	$N + N + M \rightarrow N_2 + M$	5.0×10^{15}	1.0	0
R10[f]	$C + N_2 \rightarrow CN(B) + N$	6.3×10^{13}	0	2.32×10^4
R11[f]	$C + N + M \rightarrow CN(B) + M$	3.4×10^{15}	1.0	0
R12[e]	$CN(B) + M \rightarrow CN + M$	6.0×10^{12}	0	0
R13[g]	$CN + M \rightarrow C + N + M$	2.5×10^{14}	0	7.10×10^4
	OH Emission Chemistry			
R14	$H_2O + M \rightarrow OH + H + M$	3.5×10^{15}	0	5.29×10^4
R15[g]	$OH + M \rightarrow O + H + M$	2.4×10^{15}	0	5.00×10^4
R16[f]	$O + H + M \rightarrow OH(A) + M$	1.6×10^{16}	1.0	0
R7[e]	$OH(A) + M \rightarrow OH + M$	6.0×10^{12}	0	0

[a] Unless otherwise noted, rate constants from NIST database.[20] [b] Units of A are s^{-1} (unimolecular), cm^3/(mol s) (bimolecular), and cm^6/(mol^2 s) (termolecular). [c] $k = A(298/T)^N \exp(-E/T)$. [d] See Grebe and Homann.[21] [e] Estimated at ≈1/100th gas kinetic. [f] Upper limit estimate of excited state formation rate, since all reactions are assumed to produce electronic excitation. [g] Same rate constant assumed for CN(B) and OH(A) collisional dissociation.

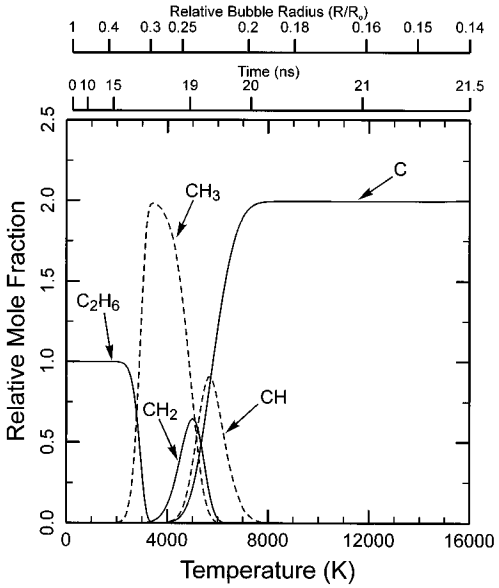

Figure 1. Model-predicted temperature/temporal concentration profiles for the decomposition of C_2H_6 seeded into an Ar bubble. The species mole fractions are normalized to the initial C_2H_6 mole fraction of 10^{-4}.

temperature dependent rate constants are given in Table 1. Although several bimolecular $C_2(d)$ production reactions have been proposed,[3] the currently favored pathway,[21] $C + CH_2 \rightarrow C_2(d) + H_2$, was selected for consideration in this study. The C_2 emission chemistry is an example of a single bond mechanism since the immediate molecular precursor to $C_2(d)$ formation, CH_2, contains only C−H single bonds.

The calculated mole fractions of the major C-containing species, normalized to an initial C_2H_6 mole fraction of 10^{-4}, are displayed in Figure 1 as a function of bubble collapse temperature (the collapse time and relative bubble radius are also indicated). The decomposition of the seed hydrocarbon molecule occurs suddenly, over a very narrow temperature interval in the vicinity of ≈3000 K. The subsequent dehydrogenation reactions, $CH_3 \rightarrow CH_2 \rightarrow CH \rightarrow C$, occur over a much broader temperature regime, approximately 3000−7000 K. Above 8000 K, complete dissociation of all C−C and C−H bonds will have been achieved. The production of electronically excited $C_2(d)$ depends on the product of the C and CH_2 concentrations, which from Figure 1 is seen to occur over a narrow temperature interval centered at 5200 K. The model calculated peak C_2 emission temperature and the narrowness of the distribution of emission temperatures are in excellent agreement with the experimentally derived[3,4] temperature(s) of 5075 ± 156 K. It is interesting to note the time intervals over which the various chemical steps occur. All of the single bond chemistry takes place in a narrow time window of ≈5 ns (this corresponds to the 3000−8000 K temperature range and a relative bubble radius range of approximately $R/R_0 = 0.3-0.19$), and the $C_2(d)$ production and emission processes occur over an even narrower time window of ≈0.5 ns.

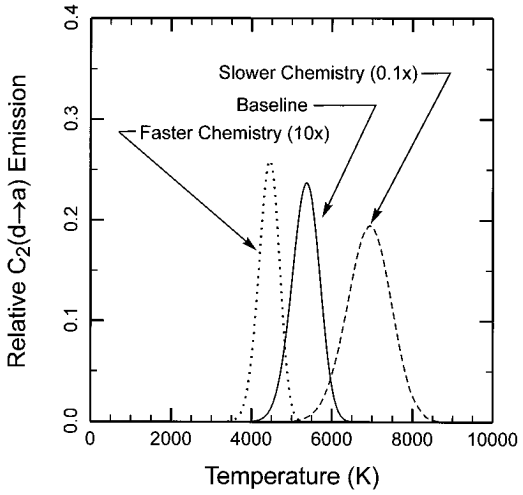

Figure 2. Model-predicted sensitivity of the $C_2(d \rightarrow a)$ temperature emission profile to variations in the chemical and dynamical time scales. A factor of 10 increase (10×) and a factor of 0.1 decrease (0.1×) in the dynamical time scale relative to the baseline are shown.

The cavitational collapse temperature/time interval over which the C_2 emission occurs is shown in Figure 2. Because of the high temperatures and densities existing within the bubble during the C_2 emission time window, the collisional dissociation and quenching rates of the electronically excited $C_2(d)$ are much greater than the radiative decay rate. In this limit, the total bubble C_2 emitted power will be directly proportional to the product of the precursor C and CH_2 mole fractions. The sensitivity of the C_2 emission to variations in the key chemical and dynamical parameters dR/dt and R_0, and the temperature dependent reaction rate constants $k(T)$, is also presented in Figure 2. Individually increasing dR/dt or R_0 by a factor of 10 is equivalent to multiplying all the reaction rate constants by a factor of 0.1 (this is labeled as 0.1× Slower Chemistry in Figure 2). Similarly, decreasing dR/dt or R_0 by a factor of 10 is equivalent to multiplying the rate constants by a factor of 10 relative to their baseline values (labeled as 10× Faster Chemistry in Figure 2). From Figure 2, it is seen that the peak location and width of the C_2 emission varies only mildly for a 2 order of magnitude variation in dR/dt, R_0, or $k(T)$; this supports the earlier assertion that the salient features of the molecular emission chemistry are only mildly dependent on the details of the dynamical model.

B. CN(B→X) SL Chemistry and Spectral Analysis. As demonstrated by Flint and Suslick,[3,22] the addition of N_2 to an Ar/hydrocarbon system produces an additional MBSL molecular emission due to CN(B→X), as shown in Figure 3. Model

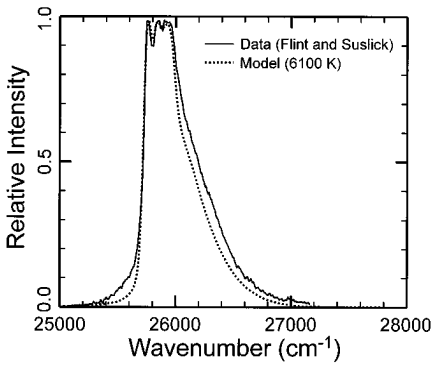

Figure 3. Comparison of single temperature synthetic spectral calculation to the observed CN(B→X) MBSL spectrum[22] for Ar/N_2 in silicone oil. The computed spectrum was degraded to the experiment resolution of 55 cm^{-1}.

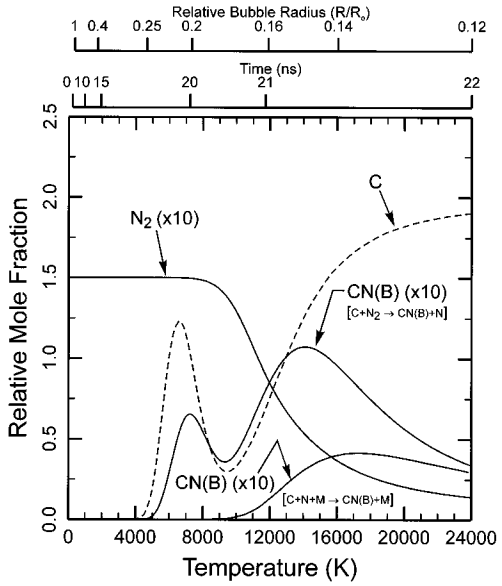

Figure 4. Model-predicted temperature/temporal concentration profiles normalized to the initial C_2H_6 mole fraction of 10^{-4} for the CN emission chemistry. For display purposes, the N_2 and CN(B) mole fractions have been multiplied by a factor of 10.

predictions of the CN emission temperature time lines for the postulated SL mechanisms are shown in Figure 4, and correspond to the same baseline conditions as previously detailed for the C_2 emission with the addition of an 0.15 N_2 mole fraction to the Ar bubble. The carbon-containing-species mole fractions have been normalized to an initial C_2H_6 mole fraction of 10^{-4}. The same proposed CN(B) formation pathways considered by Flint and Suslick are also considered here. The temperature/temporal CN(B) emission profiles for these mechanisms are directly proportional to the CN(B) mole fraction profiles also indicated in Figure 4. Both pathways produce emission at much higher temperatures and over a much broader temperature range than found for the C_2 emission. This is not surprising since one mechanism involves a triply bonded N_2 precursor and the other involves atom−atom recombination.

1. CN(B→X) SL Spectral Analysis. Initial attempts[4,22] to deduce a single effective cavitational collapse temperature from synthetic spectral modeling of the observed CN SL spectrum proved unsatisfactory. Consideration was also given to the possibility of nonequilibration of the effective rotational and vibrational temperatures; however, this did not yield a substantially improved fit to the data. An improved spectral analysis is reported here which incorporates both the effects of pressure broadening and a distribution of emission temperatures into the previously developed spectral model. For simplicity, it was assumed that both the rotational and vibrational temperatures are equilibrated to the instantaneous bubble gas kinetic temperature T. The validity of this assumption will be explored below. The effect of pressure broadening was included by spectrally distributing each emission line according to the Lorentz line shape function,[23]

$$f(\nu-\nu_i) = \frac{1}{\pi}\frac{\gamma}{\{\nu-\nu_i\}^2+\gamma^2} \tag{12}$$

where ν_i is the line-center frequency of the ith emission line and γ is the pressure-broadened line width. The line width was assumed to scale with the bubble temperature and pressure via[23]

$$\gamma = \gamma_0 \frac{P}{P_0}\left\{\frac{T_0}{T}\right\}^{1/2} \tag{13}$$

where the reference conditions were taken to be $T_0 = 300$ K and $P_0 = 1$ atm. The reference line width γ_0 was adjusted in order to fit the observed spectrum. The influence of pressure broadening is most clearly evident in the frequency region just below the band edge at ≈25 600 cm^{-1} (see Figure 3) where the emission tail is entirely due to the accumulated Lorentz wings of lines centered above 25 600 cm^{-1}. It is noted that the C_2 SL spectrum[3] does not show evidence of significant pressure broadening, consistent with the notion that the CN emission occurs at a later stage of bubble collapse corresponding to higher temperatures and pressures.

We first revisited the possibility of obtaining a satisfactory single temperature fit when the effects of pressure broadening were included. The result is shown in Figure 3 for $T = 6100$ K, $P = 2$ kbar, and $\gamma = 15$ cm^{-1} ($\gamma_0 = 0.035$ cm^{-1}). Improvements to the poor fit in the band wings can be obtained by increasing the line width; however, the quality of the fit in the peak region is then significantly degraded. This implies that at least two pressure/temperature spectral basis functions are required to obtain a good overall fit: a lower pressure/temperature curve to reproduce the well-resolved structure in the peak region and a higher pressure/temperature curve to account for the band wings. In reality, a continuous distribution of pressure/temperature spectral curves contribute to the observed spectrum; for simplicity, two spectral basis functions were used in order to estimate the range of temperatures over which the CN emission occurs. The resolution and structure of the features in the peak region require that the temperature T_1 and line width γ_1 for the lower temperature basis function be close to those for the best single basis function fit determined above. Given initial estimates for T_1 and γ_1, the temperature T_2 for the higher temperature basis function is then adjusted to yield a good fit to the spectrum. The line width γ_2 is fixed by the values of T_1, γ_1, and T_2 via the equation of state eq 4 and the line width scaling function eq 13. For a given pair of basis functions, the relative contribution of each is adjusted to yield an optimized fit. A typical fit is shown in Figure 5 for $T_1 =$ 5500 K, $P_1 = 1.5$ kbar, $\gamma_1 = 12$ cm^{-1}, $T_2 = 14\,000$ K, $P_2 = 16$ kbar, and $\gamma_2 = 81$ cm^{-1} ($\gamma_0 = 0.035$ cm^{-1} for both sets of conditions and the pressure is determined by the equation of state). Comparable fits were also obtained for ≈±10% variations in each of the quoted parameter values. The relative contributions of the colder and hotter components are comparable, a strong indication that the CN emission occurs over a broad range of cavitation temperatures, approximately 5000−15 000 K. The uncertainties in the parameter values associated with the fit do not alter this conclusion. It should be noted that

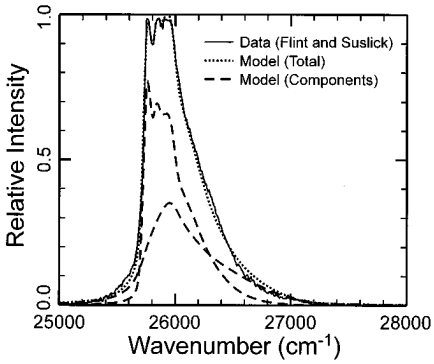

Figure 5. Comparison of two temperature synthetic spectral calculation to the observed CN(B→X) MBSL spectrum[22] for Ar/N_2 in silicone oil. The model temperatures are 5500 K (taller/narrower component) and 14 000 K (shorter/wider component).

the CN emission may persist to temperatures above 15 000 K; however, from Figure 4, it is apparent that the time-integrated emission contribution from these higher temperatures is rapidly decreasing and thus difficult to extract from the observed spectrum.

The colder temperature component is lower than expected on the basis of the reactions discussed above, and may be indicative of an additional pathway. A candidate reaction is $C_2(d) + N_2 \rightarrow CN(B) + CN$, which is mildly endothermic ($\Delta H \approx 12\,000$ K) relative to the bubble gas temperature at $T \approx 5500$ K. This is consistent with the $C_2(d)$ production reaction which turns on (and off) at ≈5100 K; however, once produced, the CN emission may, depending on the rate of quenching of the emitting molecules, persist to higher temperatures than the C_2 emission.

2. Rotational and Vibrational Relaxation. It has been previously suggested[24] that the rotational and vibrational state distributions of the emitting molecules may not always be equilibrated to the instantaneous cavitational collapse gas kinetic temperature *T*. This issue is explored more quantitatively here by comparing estimates of the rotational and vibrational relaxation time scales for representative bubble collapse conditions to the time scales for cavitational collapse and radiative decay. Full equilibration to *T* is obtained when the relaxation time scales for the nascent rotational and vibrational distributions of the initially formed emitting molecules are faster than the time scales for both cavitational collapse and radiative decay. From the cavitational collapse time scale presented earlier (see Figure 1), we estimate that in order for the rotational and vibrational temperatures to track *T* to within ≈10% or better the relaxation time scales must be of order $\Delta T \leq 0.1$ ns. It is noted that this time scale is much faster than typical intrinsic (i.e., nonquenched) radiative lifetimes which, for example, are 170 ns for C_2(d→a) and 60 ns for CN(B→X). Due to electronic quenching, the effective radiative lifetime will be much faster than the intrinsic radiative lifetime. For example, the narrowness of the derived temperature distribution for the C_2 emission places an upper bound of ≈0.5 ns on its effective radiative lifetime. As a first step in the estimation of the rotational and vibrational relaxation time scales, we consider the number of gas kinetic (i.e., hard sphere) collisions, *N*, an electronically excited molecule experiences during a specific time scale Δt. This is given by

$$N = \rho\sigma^2(8\pi k_B T/\mu)^{1/2}\Delta t \qquad (14)$$

where k_B is the Boltzmann constant and μ is the reduced mass of the colliding species. Taking the representative bubble conditions during molecular emission to be $\rho = 2 \times 10^{21}$ cm^{-3} ($\rho^* = 0.07$ for Ar), $T = 6000$ K, $\sigma = 3.5 \times 10^{-8}$ cm (representative of Ar−C_2 and Ar−CN collisions), $\mu = 15$ amu, and $\Delta t = 0.1$ ns yields $N = 220$. Since significant rotational relaxation/energy exchange will occur for each hard sphere collision, it is estimated that complete rotational equilibration to *T* will occur in about 10 hard sphere collisions, corresponding to a time scale of 0.005 ns. Previous theoretical and experimental studies[25−28] of high-temperature single quantum quenching/excitation rates of diatomics by Ar indicate that anywhere from 10 to 1000 hard sphere collisions are required for a single quenching/excitation transition to occur. It is estimated, on the basis of the exact solution for relaxation of a two-level system, that ≈4 quenching/excitation transitions are required to relax the nascent vibrational distribution to within a few percent of *T*; thus, the vibrational relaxation time scale ranges from 0.02 to 2 ns. This estimate of the vibrational relaxation time scale does not include the effects of multiquantum transitions or three-body collisional relaxation, both of which are expected to be significant and result in a reduction of the timescale.

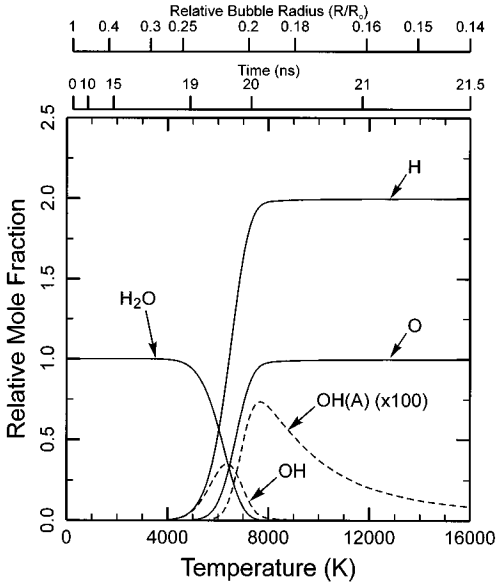

Figure 6. Model-predicted temperature/temporal concentration profiles normalized to the initial H_2O mole fraction of 10^{-2} for the OH emission chemistry. For display purposes, the OH(A) mole fractions have been multiplied by a factor of 100.

The estimated rotational and vibrational relaxation time scales support the following conclusions: (1) it is generally valid to assume that the rotational temperature is equilibrated to *T* and (2) vibrational equilibration to *T* may or may not occur, depending on the identities of both the emitting and quenching species. Thus, while fitting of molecular SL may require the use of separate rotational and vibrational temperatures (or temperature distributions), it is the deduced rotational temperature(s) that is (are) most directly indicative of the cavitational collapse temperature(s).

C. OH(A→X) SL Chemistry. MBSL emission from OH is typically the dominant molecular emission feature observed when sonication is performed in liquid H_2O.[9,18] Previous investigations of OH(A→X) emission in flames[29,30] have led to the identification of two three-body recombination pathways, $OH + OH + H \rightarrow OH(A) + H_2O$ and $O + H + M \rightarrow OH(A) + M$. From consideration of the relative concentrations of the precursors, it is expected that the latter reaction will be the dominant SL pathway. Model predictions for the OH chemistry are shown in Figure 6, and correspond to the C_2 chemistry baseline conditions with addition of a 10^{-2} H_2O mole fraction. The species mole fractions have been normalized to the initial

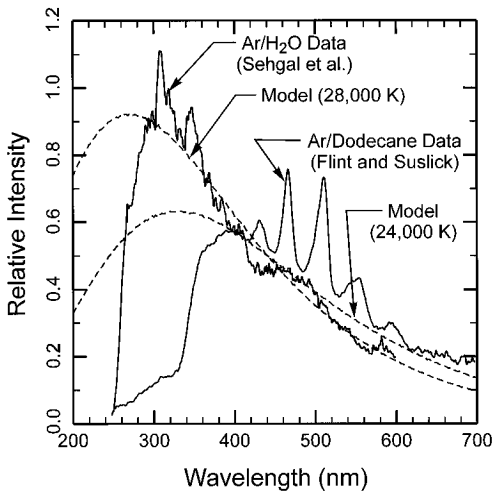

Figure 7. Comparison of model-computed spectra using the confined-electron continuum emission SL model[8] to experimentally observed MBSL spectra for the Ar/H_2O[18] and Ar/dodecane[3] systems.

H_2O mole fraction. An effective OH emission temperature of ≈8000 K is inferred for the dominant SL mechanism. The other SL pathway yields a substantially lower emission temperature of ≈6000 K due to dissociative depletion of the OH precursor. The currently available OH emission spectra are not at sufficient spectral resolution to enable a useful determination of the effective emission temperature. For the atom−atom recombination reaction, the intensity of the OH emission is proportional to the square of the initial H_2O mole fraction (H_2O is the source of the O and H atoms); therefore, the OH emission will be fairly sensitive to the liquid temperature, which determines the partial pressure of gaseous H_2O within the bubble.

We note that Kamath et al.[13b] have explored a detailed bubble collapse/chemical kinetic model for OH production under much milder collapse conditions (OH(A) production and quenching chemistry was not included). At the highest peak collapse temperature of 2900 K considered in their study, the predicted OH mole fraction relative to the initial H_2O bubble concentration was 0.014. This is consistent with the current study in which a higher bubble wall collapse velocity pushes the onset of OH formation to a higher temperature of approximately 4000 K.

D. Continuum Emission. Both SBSL and MBSL spectra display broad emission continua which generally extend throughout the ≈200−700 nm spectral region, and peak below (usually well below) 400 nm. A previous analysis[8] of the rare gas SBSL spectra yielded continuum emission temperatures of 20 000−30 000 K for Xe, 30 000−40 000 K for Ar, and 45 000−60 000 K for He. Several MBSL observations are considered here to demonstrate the similarity between the SBSL and MBSL continuum emissions. Figure 7 presents comparisons of experimental and modeled spectra for Ar/dodecane[3] and Ar/H_2O[18] MBSL experiments. The confined-electron spectral model[8] used to compute emission continua is based on three variables: the mean box size (i.e., fluid void dimension) a_0, the variance of the box size distribution α, and temperature. These variables are all directly tied to the reduced density ρ^* of the fluid inside the cavitating bubble. For the model calculations in Figure 7, the Ar/dodecane data was fit with $\rho^* = 0.50$, for which $a_0 = 7.9$ Å, $\alpha = 2.5$ Å, and $T = 24\,000$ K, and the Ar/H_2O data was fit with $\rho^* = 0.67$, for which $a_0 = 7.0$ Å, $\alpha = 2.0$ Å, and $T = 28\,000$ K. The steep, short wavelength dropoffs seen in both data sets are likely due to dropoffs in detector response and/or calibration uncertainties. In the Ar/H_2O MBSL data, the OH molecular emission is evident as the peak at 310 nm. The smaller peak near 350 nm may be due to overall intensity drifts arising from the small signal levels and long scan times, since it does not appear in other Ar/H_2O observations.[18] The derived continuum emission temperatures, 28 000 K for Ar/H_2O and 24 000 K for Ar/dodecane, are much higher than would be obtained from analysis of the accompanying molecular emissions and are consistent with the range of continuum emission temperatures of 35 000 ± 5000 K derived from the Ar SBSL data. It is not surprising that the MBSL continuum emission temperatures are different from each other and from the SBSL temperatures, since they represent averages over a broad distribution of experiment dependent cavitational collapse conditions.

Previously, the MBSL continuum emission has been ascribed to the same types of chemical pathways, bimolecular and termolecular reactions, that give rise to the molecular band emission.[1,3] It is unlikely that the continua have a molecular chemiluminescent origin primarily because it requires that the overall production/emission efficiency of the molecular continuum emitters be approximately several orders of magnitude greater than the efficiently produced and strongly allowed molecular band emissions. For example, it has been suggested[3] that for Ar/dodecane the continuum may arise from $CH + CH_2 \rightarrow C_2H^* \rightarrow C_2H + h\nu$, which is known to produce a broad visible continuum in low pressure flow reactors.[21] Using the experimentally inferred C_2H^* formation rate constant of 1×10^{14} cm^3/(mol s),[21] and a radiative decay rate of 1.6×10^5 s^{-1} (this is much smaller than the C_2 radiative decay rate of 6×10^6 s^{-1}), and assuming the baseline conditions and chemistry used for the C_2 emission calculations, the ratio of the integrated C_2H continuum to C_2 molecular emissions is estimated to be 0.04. This is clearly inconsistent with the data (see Figure 7) for which the ratio of the integrated continuum to the integrated C_2 emission is ≈10.

IV. Discussion

A. SL Chemistry and Temperature Regimes. Based on the chemical kinetic calculations and spectral analyses presented here and the previously reported[8] model for continuum emission from confined electrons, the following general picture of the chemistry and temperature regimes for molecular and continuum SL emerges. Consider the example of a rare gas bubble seeded with molecular species such as hydrocarbons, N_2, and H_2O. These seed molecules provide the reactive atomic and molecular precursors which give rise to the observed molecular emitters (i.e., C_2, CN, and OH). During an early stage of collapse, corresponding to a bubble temperature of approximately 3000 K, the dissociation rate of single bonds, such as C−H, C−C, and O−H, becomes appreciable. The single bond dissociation process occurs over a significant temperature/time interval because the dissociation process is controlled by finite rate chemical kinetics, and there is a significant spread in the bond energies of the seed species and their decomposition fragments. It is generally expected that complete dissociation of all single bonds will be attained when or before a temperature of ≈8000 K is reached. The dissociatively formed atomic and molecular species can participate in chemical reactions which produce electronically excited molecules, like C_2(d), which emit in the visible and ultraviolet spectral regions. Because all of the single bonds will be broken by ≈8000 K, chemiluminescent reactions involving single bond containing molecular precursors can only give rise to observable molecular emission within the 3000−8000 K temperature interval. Furthermore, the actual temperature interval characterizing a particular molecular emission is expected to be fairly narrow because it will depend on the temporal overlap of two transient species (i.e., a bimolecular

reaction) with different concentration histories. Thus, observation of molecular SL from single bond chemistry determines only a *lower* bound to the maximum caviation temperature.

Chemiluminescent reactions involving multiple bond containing species, such as triply bonded N_2, will persist to considerably higher temperatures (≈25 000 K) than single bond chemistry because of the much higher dissociation energies of multiple bonds. Chemiluminescence from atom−atom recombination chemistry (i.e., A + B + M → AB* + M) will also persist to higher temperatures than single bond chemistry; however, the recombination pathway will eventually turn off because the efficiency of three-body recombination typically decreases with an increase in temperature and the rate constant for collisional dissociation of AB* typically increases as the temperature increases.

From the preceding discussion, two generalizations can be drawn concerning the use of molecular SL to infer information about the temperatures attained during cavitational collapse: (1) different molecular emitters are expected to yield different temperatures (even when several different emitters are observed simultaneously for a given SL experiment) and (2) the temperatures derived from molecular emission are expected to fall within the ≈3000−25 000 K range. These ideas are supported by the spectral analysis described earlier of CN(B→X) MBSL which indicated that the CN emission occurs over a broad range of cavitational collapse temperatures from ≈5000 to 15 000 K. The CN emission was accompanied by C_2 emission which, as noted above, is well characterized by a single temperature of approximately 5100 K.

As the cavitational collapse proceeds beyond the molecular emission regime, the temperature becomes sufficiently high to ionize both the dissociatively formed and host rare gas atoms. The electrons produced by this ionization become confined to voids in the dense fluid formed during the latter stages of cavitational collapse. These confined electrons give rise to discrete transitions in the visible and ultraviolet spectral regions which appear as an emission continuum due to the substantial spread in the void size distribution.[8] Electrons, unlike molecules, do not dissociate or ionize as the temperature is increased; thus, the continuum emission can track the cavitation temperature over a much wider and higher temperature range (≈20 000−100 000 K) than the molecular emission.

B. MBSL and SBSL Spectral Features. In the Introduction it was noted that SBSL spectra appear to consist of only continuum emission, where as MBSL spectra generally exhibit both continuum and molecular band emissions. The SL chemistry discussed here offers a simple explanation of this observation. The confined electrons which give rise to the continuum SL are much more efficient emitters than the electronically excited molecules which give rise to the molecular SL. A representative Einstein *A* coefficient for a confined electron is $\approx 1 \times 10^9\ s^{-1}$.[8] This can be compared to Einstein *A* values for molecular emission of 6×10^6 (C_2(d→a)), 1.7×10^7 (CN(B→X)), and $1.4 \times 10^6\ s^{-1}$ (OH(A→X)). The much higher emission rate for a confined electron is the principal reason why the continuum is usually the dominant feature (in terms of the spectrally integrated power) in both SBSL and MBSL. For example, SBSL has been observed for rare gases in H_2O; thus, OH(A→X) molecular emission might be expected. On the basis of the above Einstein *A* coefficients, it is noted that confined electron emission is a factor of ≈700 more efficient than OH(A→X) molecular emission. Given comparable peak concentrations for the confined electrons and OH molecules for SBSL, the spectrally integrated continuum emission will be ≈700 times greater than the OH A → X molecular emission. The observation of significant molecular emission for MBSL, and not for SBSL, is postulated to be a consequence of the broad distribution of initial bubble sizes for MBSL.[1] In SBSL, a single bubble is repetitively cycled through collapse and reexpansion, and its collapse is driven well into the continuum emission regime. In MBSL, only a small fraction of the bubbles will be driven to this level of collapse, while a much larger fraction will attain only the single or multiple bond chemistry regimes. Thus in MBSL the bubble size distribution averaged emission will tend to enhance the molecular relative to the continuum emission.

C. SL from Atomic Emission Lines. The current study has focused on molecular SL because SL from atomic emission lines is not as ubiquitous as one might expect. Atomic emission lines have been observed only for MBSL in which high concentrations of metal carbonyls[31,32] or alkali metal salts[33] have been dissolved in the liquid. For the alkali metal salt experiments, it appears that the atomic SL occurs only in the liquid region surrounding the collapsing bubble. For the metal carbonyls, which have much higher vapor pressures than the alkali metal salts, it appears that the atomic SL occurs within the collapsing bubble. For the more commonly present MBSL and SBSL atomic species, including the rare gases, C, N, O, and H, not a single atomic emission line has been observed. For the rare gases, the most intense emission line would be for the transition between the lowest excited state and the ground state.[34] In all cases, this line falls below the 200 nm short wavelength detection cutoff for previous MBSL and SBSL experiments. Transitions between excited states can fall within the 200−700 nm observation window; however, these transitions are much weaker than that from the lowest excited state because they originate from much higher energy levels and thus have much smaller populations and/or much smaller Einstein *A* coefficients.[34] Similar considerations indicate that atomic emission lines from C, N, O, and H would also be difficult to observe, particularly when these species are present as minor constituents in rare gas bubbles.

V. Conclusions

A coupled model of the bubble dynamics and chemical kinetics of the cavitational collapse process has been developed and used to explore the chemical origins and temperature/temporal behaviors of molecular and continuum SBSL and MBSL. The model appears to be consistent with many of the key experimental SBSL and MBSL spectra and supports the following general conclusions: (1) The underlying physical mechanism for molecular and continuum MBSL and SBSL is consistent with compressional heating from adiabatic cavitational collapse of the bubble wall. (2) Molecular SL arises from chemiluminescent reactions between atomic and molecular decomposition species formed by thermal dissociation of parent molecules. (3) Different chemiluminescent reactions may occur at different times during cavitational collapse and thus give rise to emission spectra characterized by different temperatures and pressures. (4) The chemiluminescent pathways may be broadly characterized as arising from reactions involving singly or multiply bonded molecular precursors with corresponding effective emission temperatures in the ranges of ≈3000−8000 K and ≈8000−25 000 K, respectively. (5) The strong continuum emission observed in most MBSL and all SBSL experiments arises from electrons produced by high-temperature ionization and confined to voids formed in the dense fluid during the later stages of bubble collapse; the continuum is characterized by emission temperatures in the ≈20 000−100 000 K range.

(6) The differences between MBSL and SBSL spectra are attributed to the broad distribution of initial bubble sizes for MBSL.

Acknowledgment. This effort was supported by Spectral Sciences, Inc., and the National Science Foundation. The authors thank Dr. M. Bernstein, Dr. S. Adler-Golden, Dr. Y. Didenko, and Professor J. Lisy for helpful technical discussions and Dr. S. Richtsmeier for preparation of the artwork.

References and Notes

(1) Walton, A. J.; Reynolds, G. T. *Adv. Phys.* **1984**, *33*, 595.
(2) Suslick, K. S.; Doctycz, S. J.; Flint, E. B. *Ultrasonics* **1990**, *28*, 280.
(3) Flint, E. B.; Suslick, K. S. *J. Am. Chem. Soc.* **1989**, *111*, 6987.
(4) Flint, E. B.; Suslick, K. S. *Science* **1991**, *253*, 1397.
(5) Crum, L. A. *Phys. Today* **1994**, *47*, 22.
(6) Misik, V.; Miyoshi, N.; Riesz, P. *J. Phys. Chem.* **1995**, *99*, 3605.
(7) Hiller, R.; Wenninger, K.; Putterman, S. J.; Barber, B. P. *Science* **1994**, *266*, 248.
(8) Bernstein, L. S.; Zakin, M. R. *J. Phys. Chem.* **1995**, *99*, 14619.
(9) Didenko, Y. T.; Pugach, S. P. *J. Phys. Chem.* **1994**, *98*, 9742.
(10) Crum, L. A.; Roy, R. A. *Science* **1994**, *266*, 233.
(11) Gaitan, D. F.; Crum, L. A.; Roy, R. A.; Church, C. C. *J. Acoust. Soc. Am.* **1992**, *91*, 3166.
(12) Löfstedt, R.; Barber, B. P.; Putterman, S. J. *Phys. Fluids* **1993**, *A5*, 2911.
(13) (a) Frommhold, L.; Atchley, A. A. *Phys. Rev. Lett.* **1994**, *73*, 2883. (b) Kamath, V.; Prosperetti, A.; Egolfopoulos, F. N. *J. Acoust. Soc. Am.* **1993**, *94*, 248.
(14) Hiller, R.; Putterman, S. J.; Barber, B. P. *Phys. Rev. Lett.* **1992**, *69*, 1182.
(15) Wu, C. C.; Roberts, P. H. *Phys. Rev. Lett.* **1993**, *70*, 3424.
(16) Moss, W. C.; Clarke, D. B.; White, J. W.; Young, D. A. *Phys. Fluids* **1994**, *6*, 2979.
(17) Matula, T. J.; Roy, R. A.; Mourad, P. D.; McNamara, W. B., III; Suslick, K. S. *Phys. Rev. Lett.* **1995**, *75*, 2602.
(18) Sehgal, C.; Sutherland, R. G.; Verall, R. E. *J. Phys. Chem.* **1980**, *84*, 388.
(19) Carnahan, N. F.; Starling, K. E. *J. Chem. Phys.* **1969**, *51*, 635.
(20) Westley, F.; Herron, J. T.; Cvetanovic, R. J.; Hampson, R. F.; Mallard, W. G., Eds. *NIST Chemical Kinetics Data Base*; U.S. Department of Commerce: Washington, DC, 1990.
(21) Grebe, J.; Homann, K. H. *Ber. Bunsen-Ges. Phys. Chem.* **1982**, *86*, 587.
(22) Flint, E. B. Spectroscopic Studies of Sonoluminescence. Ph.D. Thesis, University of Illinois at Urbana−Champaign, 1990.
(23) Penner, S. S. *Quantitative Molecular Spectroscopy and Gas Emissivities*; Addison-Wesley: London, 1959; p 31.
(24) Jeffries, J. B.; Copeland, R. A.; Suslick, K. S.; Flint, E. B. *Science* **1992**, *256*, 248.
(25) Millikan, R. C.; White, D. R. *J. Chem. Phys.* **1963**, *39*, 3209.
(26) Wray, K. L. *J. Chem. Phys.* **1962**, *36*, 2597.
(27) Kamimoto, G.; Matsui, H. *J. Chem. Phys.* **1970**, *53*, 3987.
(28) Seary, D. J. *J. Chem. Phys.* **1973**, *58*, 1796.
(29) Hidaka, Y.; Takahashi, S.; Kawano, H.; Suga, M.; Gardiner, W. C., Jr. *J. Phys. Chem.* **1982**, *86*, 1429.
(30) Davis, M. G.; McGregor, W. K.; Mason, A. A. *J. Chem. Phys.* **1974**, *61*, 1352.
(31) Suslick, K. S.; Flint, E. B.; Grinstaff, M. W.; Kemper, K. A. *J. Phys. Chem.* **1993**, *97*, 3098.
(32) Suslick, K. S.; Kemper, K. A. In *Bubble Dynamics and Interface Phenomena*; Blake, J. R., et al., Eds.; Kluwer Academic Press: Netherlands, 1993; pp 34−39.
(33) Suslick, K. S.; Flint, E. B. *J. Phys. Chem.* **1991**, *95*, 1484.
(34) Reader, J.; Corliss, C. H.; Wiese, W. L.; Martin, G. A. *Wavelengths and Transition Probabilities*; NSRDS-NBS 68; U.S. Government Printing Office: Washington, DC, 1980.

JP953643N